ELSEVIER

Journal of Contaminant Hydrology 31 (1998) 1–21

JOURNAL OF
Contaminant
Hydrology

Contaminant transport resulting from multicomponent nonaqueous phase liquid pool dissolution in three-dimensional subsurface formations

Constantinos V. Chrysikopoulos *, Kenneth Y. Lee

Department of Civil and Environmental Engineering, University of California, Irvine, CA 92697-2175, USA

Received 29 January 1997; revised 30 May 1997; accepted 30 May 1997

Abstract

A semi-analytical method for simulating transient contaminant transport originating from the dissolution of multicomponent nonaqueous phase liquid (NAPL) pools in three-dimensional, saturated, homogeneous porous media is presented. Each dissolved component may undergo first-order decay and may sorb under local equilibrium conditions. The NAPL pool dissolution process is envisioned to occur in a series of consecutive short intervals (pulses). The mole fraction, nonaqueous phase activity coefficient and aqueous solubility of every pool constituent are estimated before the initiation of each pulse, and they are assumed to remain constant for the duration of each interval. Individual component aqueous phase concentrations resulting from each dissolution interval are estimated by existing analytical solutions applicable to single component NAPL pools, and total concentration distributions of the same component are obtained by direct superposition. The semi-analytical method is more efficient and less computationally demanding than a finite-difference approximation. Furthermore, it is shown that neglecting the changes in nonaqueous phase activity coefficients that occur during multicomponent NAPL pool dissolution may result in erroneous predictions. The model presented in this work is useful for the design and interpretation of experiments in laboratory bench scale aquifers, certain homogeneous subsurface formations, and for the verification of complex numerical codes. © 1998 Elsevier Science B.V.

1. Introduction

The accidental release of nonaqueous phase liquids (NAPLs), such as petroleum hydrocarbons and organic solvents, into the subsurface environment is a widespread

* Corresponding author.

PII S0169-7722(97)00053-3

problem that motivates this work. NAPLs may exist in unsaturated as well as saturated formations in the form of entrapped ganglia (blobs) and pools. Ganglia are retained by capillary forces, whereas pools of NAPLs lighter than water are formed above the water table, and pools of NAPLs denser than water are formed onto formation layers of low permeability (Schwille, 1988). Many common NAPLs have very low aqueous solubilities, thus they may serve as long-term sources of groundwater contamination. Furthermore, NAPL pools resist dissolution substantially longer than ganglia due to their lower NAPL–water interfacial area (Anderson et al., 1992).

There are several studies available in the literature focusing on the migration of NAPLs and dissolution of residual blobs (Abriola and Pinder, 1985; Pantazidou and Sitar, 1993; Geller and Hunt, 1993; Lenhard et al., 1993; Imhoff et al., 1994; Powers et al., 1994; Mayer and Miller, 1996, to mention a few), as well as pool dissolution (Anderson et al., 1992; Johnson and Pankow, 1992; Chrysikopoulos et al., 1994; Pearce et al., 1994; Seagren et al., 1994; Voudrias and Yeh, 1994; Whelan et al., 1994; Chrysikopoulos, 1995; Lee and Chrysikopoulos, 1995; Holman and Javandel, 1996; Mason and Kueper, 1996). In spite of the fact that the majority of groundwater contamination sites involve multicomponent NAPLs, most of the theoretical and experimental studies are focused on single-component systems. In particular, the literature on multicomponent NAPL pool dissolution is rather limited.

In this paper, we study the multicomponent transport of contaminants originating from the dissolution of NAPL pools in saturated porous media. The pool is assumed to be formed at the interface between a homogeneous sand formation and a low permeability clay layer. A semi-analytical procedure is introduced. The method assumes that the contaminant source input can be represented by a series of consecutive short pulses. For the duration of each pulse, the equilibrium aqueous solubility of every pool constituent is considered invariant. The mole fraction, nonaqueous phase activity coefficient, and consequently, the aqueous solubility of every pool constituent are updated before each pulse period. The procedure is illustrated for a hypothetical site contaminated by three NAPL pools consisting of 1,1,2-trichloroethane (1,1,2-TCA) and trichloroethylene (TCE) mixtures.

The modeling approach adopted in this work is a substantial extension to earlier work by Lee and Chrysikopoulos (1995). The physical model is improved by accounting for shrinkage of the NAPL–water interface and shifting of the pool center in the downstream direction. This progressive reduction of the NAPL pool surface area is modeled as a time dependent NAPL–water interfacial boundary. In addition, a semi-analytical method of solution is employed instead of a numerical approximation. Furthermore, a considerably extensive discussion of the fundamental model assumptions is provided.

2. Theory

2.1. Model formulation and assumptions

Consider a multicomponent NAPL pool that is denser than water formed on top of a low permeability layer within a three-dimensional, saturated, homogeneous and isotropic

porous medium. The transient transport of each dissolving component under steady-state uniform flow conditions is governed by

$$R_p \frac{\partial C_p(t,x,y,z)}{\partial t} = D_{x_p} \frac{\partial^2 C_p(t,x,y,z)}{\partial x^2} + D_{y_p} \frac{\partial^2 C_p(t,x,y,z)}{\partial y^2} + D_{z_p} \frac{\partial^2 C_p(t,x,y,z)}{\partial z^2} - U_x \frac{\partial C_p(t,x,y,z)}{\partial x} - \lambda_p R_p C_p(t,x,y,z), \quad (1)$$

where $C(t,x,y,z)$ is the liquid phase solute concentration; x, y, z are the spatial coordinates in the longitudinal, lateral and vertical directions, respectively; t is time; R is the dimensionless retardation factor; D_x, D_y, D_z are the longitudinal, lateral and vertical hydrodynamic dispersion coefficients, respectively; U_x is the average interstitial fluid velocity; λ is a first-order decay constant; and subscript p is the component number indicator. For mathematical simplicity, it is hypothesized that the sorption of each dissolved component is based on linear equilibrium isotherm, and that the local chemical equilibrium assumption is valid. The decay term λRC in the governing Eq. (1) indicates that the total concentration of a component (aqueous plus sorbed solute mass) may diminish due to possible biological/chemical degradation. The hydrodynamic dispersion coefficients and the unidirectional fluid velocity are considered constant with respect to time and space. These assumptions are necessary for analytical or semi-analytical modeling and have been used extensively in the literature for various contaminant transport applications (e.g., Hunt, 1978; Wilson and Miller, 1978; Goltz and Roberts, 1986; Leij et al., 1991, 1993; Batu, 1996; Bosma et al., 1996).

As the NAPL pool dissolves into the aqueous phase, a concentration boundary layer for each component is developed above the NAPL–water interface. Furthermore, for a NAPL pool with insignificant thickness relative to the thickness of the aquifer, the transfer of each component from the NAPL–water interface to the interstitial fluid is described by the following mass transfer relationship (Chrysikopoulos et al., 1994)

$$-\mathscr{D}_{e_p} \frac{\partial C_p(t,x,y,0)}{\partial z} = k_p(t,x,y)\left[C_p^{w}(t) - C_p(t,x,y,\infty)\right], \quad (2)$$

where $\mathscr{D}_{e_p} = \mathscr{D}_p/\tau^*$ is the effective molecular diffusion coefficient of component p; $\mathscr{D}$ is the molecular diffusion coefficient; τ^* is the tortuosity coefficient ($\tau^* \geq 1$); $k(t,x,y)$ is the local mass transfer coefficient dependent on time and location at the NAPL–water interface; and $C^{w}(t)$ is the equilibrium aqueous solubility that is time-dependent because the mole fraction of each component is changing as the NAPL dissolves into the aqueous phase. It should be noted that $C_p(t,x,y,\infty)$ is the bulk or background concentration of component p in the interstitial fluid. Conventionally, any location above the concentration boundary layer is considered as $z \to \infty$. For the case where the background concentration is constant with respect to time and space, for notational convenience, $C_p(t,x,y,\infty)$ is replaced by C_{b_p} where C_b is the constant background liquid

phase concentration. The left-hand side term in Eq. (2) represents the diffusive flux into the boundary layer at the NAPL–water interface given by Fick's law, whereas the right-hand side represents the convective mass transfer flux. Convective mass transfer occurs when $C_p(t,x,y,0) \neq C_p(t,x,y,\infty) = C_{b_p}$, and is analogous to Newton's law of cooling (Bird et al., 1960; p. 267). The mass transfer expression (Eq. (2)) has been applied in numerous engineering applications such as: evaporation of a flat surface (Crank, 1975; p. 60); dissolution of a soluble plate in laminar flow (Weber and DiGiano, 1996; p. 202), dissolution of NAPL pools in porous formations (Chrysikopoulos, 1995), NAPL removal by soil venting (Lingineni and Dhir, 1997), among others.

There are several important assumptions embodied in the mass transfer relationship (Eq. (2)). The dissolution at the NAPL–water interface is fast, so the liquid phase solute concentration is not limited by the NAPL pool dissolution, only by the mass transfer of the dissolved solute. The concentration of each dissolving component along the NAPL–water interface is equal to its time-dependent equilibrium aqueous solubility

$$C_p(t,x,y,0) = C_p^{\mathrm{w}}(t). \tag{3}$$

For a single component NAPL pool the concentration along the interface is constant and equal to the saturation concentration

$$C(t,x,y,0) = C_{\mathrm{s}}, \tag{4}$$

where C_{s} is the single component aqueous saturation concentration (solubility of pure component).

The development of a concentration boundary layer at steady-state uniform flow conditions for two different constant background liquid phase concentrations is shown in Fig. 1. The NAPL–water interface is indicated by the x-axis, whereas the concentration within the boundary layer is shown with arrows. Traditionally, arrows are reserved for the representation of vectors; however, arrows are used in Fig. 1 for convenient sketching of the magnitude of the scalar concentration. The first case (Fig. 1a) illustrates the situation where the background liquid phase concentration is zero and the concentration within the boundary layer decreases from saturation concentration at the NAPL–water interface to zero concentration in the bulk interstitial liquid. The second case (Fig. 1b) represents the situation where the background concentration is constant, but nonzero, and the concentration within the boundary layer varies from the solubility limit at the interface to a finite constant concentration in the bulk interstitial fluid. The thickness of the boundary layer depends mainly on the hydrodynamics and dispersion properties of the system, and is defined as the value of z for which $[C_p(t,x,y,0) - C_p(t,x,y,z)]/[C_p(t,x,y,0) - C_p(t,x,y,\infty)] = 0.99$ (Incropera and DeWitt, 1990, p. 321). Examination of Fig. 1 indicates that a thin boundary layer corresponds to steeper concentration gradients. It should be noted, however, that the greater the concentration gradient the greater the mass transfer of the dissolved component. Therefore, the local mass transfer coefficient decreases with distance from the front end of the NAPL pool, and has a maximum value at the leading or upstream edge. The local mass transfer coefficient is not only spatially but temporally dependent during the initial period of formation of the boundary layer. At steady-state physicochemical and hydrodynamic conditions, the local mass transfer coefficient is independent of time.

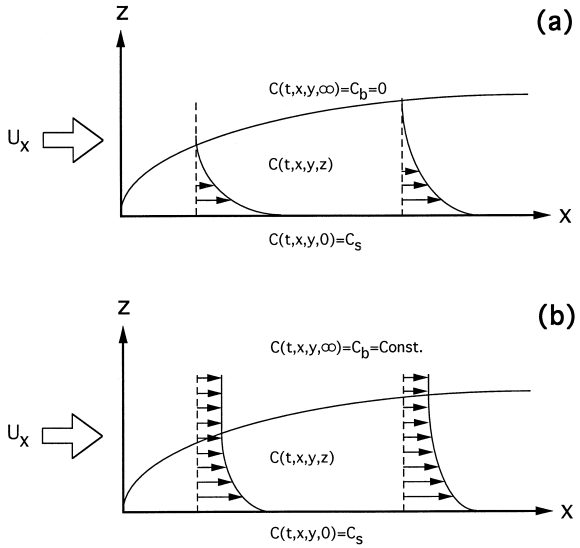

Fig. 1. Development of a concentration boundary layer along the NAPL–water interface in uniform interstitial flow for (a) zero bulk aqueous phase (background) concentration and (b) constant nonzero background concentration.

The local mass transfer coefficient can only be obtained experimentally and is case-specific. Unfortunately, the local mass transfer coefficient usually is not an easy parameter to determine with precision. Thus, in mathematical modeling of contaminant transport from NAPL pool dissolution, $k(t,x,y)$ is often replaced by the average (or overall) mass transfer coefficient, $\bar{k}(t)$, for the entire pool expressed as (Incropera and DeWitt, 1990; p. 313):

$$\bar{k}(t) = \frac{1}{A}\int_A k(t,x,y)\, d^2\boldsymbol{A}, \tag{5}$$

where A is the surface area of the NAPL pool, and $d^2\boldsymbol{A}$ is a differential surface area. At steady-state physicochemical and hydrodynamic conditions, the time invariant overall mass transfer coefficient is denoted by k^*. Certainly, for a multicomponent NAPL pool, true steady-state physicochemical conditions may never be attained, so that the average mass transfer coefficient may remain a time-dependent variable. In this work, the mathematical development is based on the assumption that the local mass transfer coefficient is equal to the corresponding time invariant overall mass transfer coefficient ($k^* = k(t,x,y)$). It should be noted that for the case of NAPL pool dissolution no applicable mass transfer coefficient correlation is reported in the literature. Conversely, theoretical and experimentally derived correlations for overall mass transfer coefficients for dissolving spherical residual NAPL blobs in packed columns are frequently presented in the literature (e.g., Imhoff et al., 1994; Powers et al., 1994; Mayer and Miller, 1996).

For a multicomponent NAPL pool with elliptic shape, constant vertical thickness, and homogeneous composition, formed above an impermeable stratum along the *xy* plane, as shown in Fig. 2, the appropriate initial and boundary conditions for each dissolving component are:

$$C_p(0,x,y,z) = C_{b_p}, \tag{6}$$

$$C_p(t,\pm\infty,y,z) = C_{b_p}, \tag{7}$$

$$C_p(t,x,\pm\infty,z) = C_{b_p}, \tag{8}$$

$$-\mathscr{D}_{e_p}\frac{\partial C_p(t,x,y,0)}{\partial z} = \begin{cases} k_p^*\left[C_p^w(t) - C_{b_p}\right] & \dfrac{\left(x-\ell_{x_o}\right)^2}{a^2} + \dfrac{\left(y-\ell_{y_o}\right)^2}{b^2} \le 1, \\ 0 & \text{otherwise}, \end{cases} \tag{9}$$

$$C_p(t,x,y,\infty) = C_{b_p}, \tag{10}$$

where ℓ_{x_o} and ℓ_{y_o} indicate the x and y Cartesian coordinates of the center of the elliptic pool, respectively; and a, b are the major and minor semi-axes of the elliptic pool, respectively. It should be noted, however, that the circular pool geometry is a special case of an elliptic pool (see Fig. 2). Therefore, the appropriate source boundary condition for a circular pool is obtained by setting $a = b = r$ in Eq. (9). It is important to clarify that the assumption of a homogeneous NAPL pool implies that no mass transfer limitations from within the NAPL occur (the diffusion of each component in the NAPL mixture is rapid relative to the pool dissolution rate). This assumption is often employed in NAPL dissolution studies reported in the literature (e.g., Mackay et al., 1991).

2.2. Multicomponent aqueous solubility

For multicomponent NAPL systems, the aqueous phase concentration of each dissolving component is controlled in part by the equilibrium aqueous solubility of each

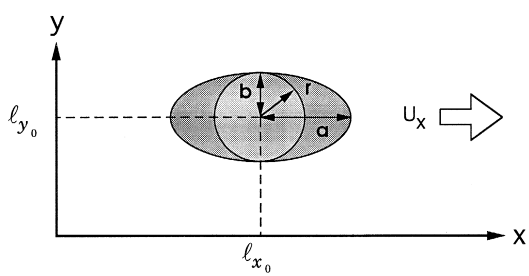

Fig. 2. Plan view of a denser than water elliptic pool with origin at $x = \ell_{x_o}, y = \ell_{y_o}$, having major semi-axis a and minor semi-axis b. For the special case where $a = b = r$, the elliptic pool becomes a circular pool with radius r.

individual component (Borden and Piwoni, 1992). The aqueous solubility is a function of the time-dependent mole fraction. As the mole fraction of each component changes constantly with a rate proportional to its mass transfer coefficient, the activity coefficient of each component is also changing accordingly (Fredenslund et al., 1977). The activity coefficient is a dimensionless correction term indicating the nonideality of a solution (Schwarzenbach et al., 1993). The higher the deviation of activity coefficients from unity, the greater the degree of nonideality of a solution.

The equilibrium aqueous solubility of component p is given by (Broholm and Feenstra, 1995; Lee and Chrysikopoulos, 1995)

$$C_p^{\mathrm{w}}(t) = C_{\mathrm{s}_p} X_p(t)\,\gamma_p(X_p), \tag{11}$$

where X is the mole fraction of component p in the nonaqueous phase; and γ is the activity coefficient in the nonaqueous phase. It should be noted that the activity coefficients are dependent on the mole fraction of component p in the nonaqueous phase.

The experimental studies conducted by Banerjee (1984) suggest that the nonaqueous phase activity coefficients for a NAPL mixture containing components of similar structure can be approximated at ideal state equal to one ($\gamma_p \simeq 1$). For this special case, Eq. (11) simply reduces to Raoult's law, and represents the situation where the NAPL mixture behaves ideally and the aqueous phase concentration of each component is equal to the single component aqueous saturation concentration multiplied by the mole fraction of the component. However, despite structural similarity, Eq. (11) should be used whenever nonaqueous activity coefficient relationships can be obtained.

For multicomponent NAPL mixtures, the nonaqueous phase activity coefficient can be estimated using the UNIFAC (UNI-Functional group Activity Coefficients) method. The UNIFAC method was initially developed by Fredenslund et al. (1975) and has since been revised as well as improved several times (Fredenslund et al., 1977; Skjold-Jørgensen et al., 1979; Gmehling et al., 1982; Macedo et al., 1983; Tiegs et al., 1987; Hansen et al., 1991). UNIFAC is a valuable semiempirical thermodynamic model for estimating liquid phase activity coefficients of nonideal liquid mixtures for which little or no experimental information exists. The model is based on the solution of groups concept, which does not consider a liquid mixture as a solution of molecules, but as a solution of groups. The advantage of this method is that the activity coefficients can be estimated for practically any organic molecule, provided that the molecule consists of structural groups for which parameters are available. The activity coefficients are determined from two parts as follows:

$$\ln \gamma_p = \ln \gamma_p^{\mathrm{C}} + \ln \gamma_p^{\mathrm{R}}, \tag{12}$$

where the first term on the right-hand side is the combinatorial part (indicated by superscript C) that takes into account differences in size and shape of the molecules in the mixture; and the second term on the right-hand side is the residual part (indicated by superscript R) which derives from intermolecular interactions (Fredenslund et al., 1975). The UNIFAC method has been employed in numerous applications of interest in

environmental engineering involving estimation of Henry's constants (Munz and Roberts, 1987) and aqueous as well as nonaqueous solubilities (Broholm and Feenstra, 1995; Lee and Chrysikopoulos, 1995; Kan and Tomson, 1996).

2.3. Semi-analytical solution

A closed-form analytical solution to the problem defined by Eq. (1) and Eqs. (6)–(10) cannot be derived, because the equilibrium aqueous solubility, C^{w}, which appears in the source boundary condition (Eq. (9)) is a time dependent parameter given by Eq. (11). However, a semi-analytical solution can be obtained by representing the source input as a summation of consecutive pulse-type boundary conditions, assuming that the NAPL pool composition, and consequently C^{w}, of each component remain constant over a 'small' time interval, Δt. For every pulse-type input the following analytical solution derived by Chrysikopoulos (1995) is applicable

$$C_p(t,x,y,z) = \begin{cases} \left[C_p^{\mathrm{w}}(t) - C_{\mathrm{b}_p}\right]\Phi_p(t,x,y,z), & 0 < t \le \Delta t, \\ \left[C_p^{\mathrm{w}}(t) - C_{\mathrm{b}_p}\right]\left[\Phi_p(t,x,y,z) - \Phi_p(t-\Delta t,x,y,z)\right], & t > \Delta t, \end{cases} \tag{13}$$

where

$$\Phi_p(t,x,y,z) = \frac{k_p^*}{2\pi\mathscr{D}_{\mathrm{e}_p}} \int_0^t \int_{\mu_1}^{\mu_2} \left(\frac{D_{z_p}}{R_p\tau}\right)^{1/2} \exp\left[-\lambda_p\tau - \frac{R_p z^2}{4D_{z_p}\tau}\right] \times \exp\left[-\mu^2\right]\left(\operatorname{erf}[n_2] - \operatorname{erf}[n_1]\right)\mathrm{d}\mu\,\mathrm{d}\tau, \tag{14}$$

where

$$\mu_1 = \left(y - \ell_{y_o} + b\right)\left(\frac{R_p}{4D_{y_p}\tau}\right)^{1/2}, \tag{15}$$

$$\mu_2 = \left(y - \ell_{y_o} - b\right)\left(\frac{R_p}{4D_{y_p}\tau}\right)^{1/2}, \tag{16}$$

$$n_1 = \left\{x - \frac{U_x\tau}{R_p} - \ell_{x_o} + \left[a^2 - \frac{a^2\left(\upsilon - \ell_{y_o}\right)^2}{b^2}\right]^{1/2}\right\}\left(\frac{R_p}{4D_{x_p}\tau}\right)^{1/2}, \tag{17}$$

$$n_1 = \left\{x - \frac{U_x\tau}{R_p} - \ell_{x_o} - \left[a^2 - \frac{a^2\left(\upsilon - \ell_{y_o}\right)^2}{b^2}\right]^{1/2}\right\}\left(\frac{R_p}{4D_{x_p}\tau}\right)^{1/2}, \tag{18}$$

$$\upsilon = y - \mu\left(\frac{4D_{y_p}\tau}{R_p}\right)^{1/2}, \tag{19}$$

where τ and μ are dummy integration variables. It should also be noted that in Eq. (13), the superposition principle is employed over the time interval Δt. Superposition is possible because the governing Eq. (1) is linear with respect to the liquid phase solute concentration.

Although the model simulations are based on a time invariant overall mass transfer coefficient (k^*), as discussed earlier, the local mass transfer coefficient decreases with distance from the leading edge of the NAPL pool in the direction of the interstitial flow. Thus, it is reasonable to assume that the majority of the dissolved mass originates from the upstream front end of the NAPL pool. In this work the NAPL pool shrinkage due to dissolution is accounted for at each time interval. Fig. 3 illustrates the surface area of NAPL pools undergoing dissolution at time t_1 and at two subsequent times, t_2 and t_3. At time t_1 the major and minor semi-axes of the elliptic pool are indicated by a_1 and b_1, respectively, the radius of the circular pool is indicated by r_1, whereas, the location of the center of the pool on the xy plane is at $x=\ell_{x_o}(t_1)$ and $y=\ell_{y_o}$. As the NAPL pool shrinks with time, the center of the pool is moving in the downstream direction ($\ell_{x_o}(t_1)<\ell_{x_o}(t_2)<\ell_{x_o}(t_3)$). Furthermore, it is assumed that there is no lateral fluctuation of the pool center, and that NAPL pool shrinkage affects the size but not the original shape or thickness of the pool. Thus, an elliptic pool is assumed to remain elliptic with constant ratio of major to minor semi-axis and a circular pool to remain circular, as shown in Fig. 3. This is an approximate model for the representation of pool shrinkage.

At the beginning of each time interval, the pool composition is updated, X and γ are evaluated accordingly, and C^w is calculated for each component by using Eq. (11). The nonaqueous phase activity coefficient, $\gamma_p(X_p)$, of component p at time t is estimated

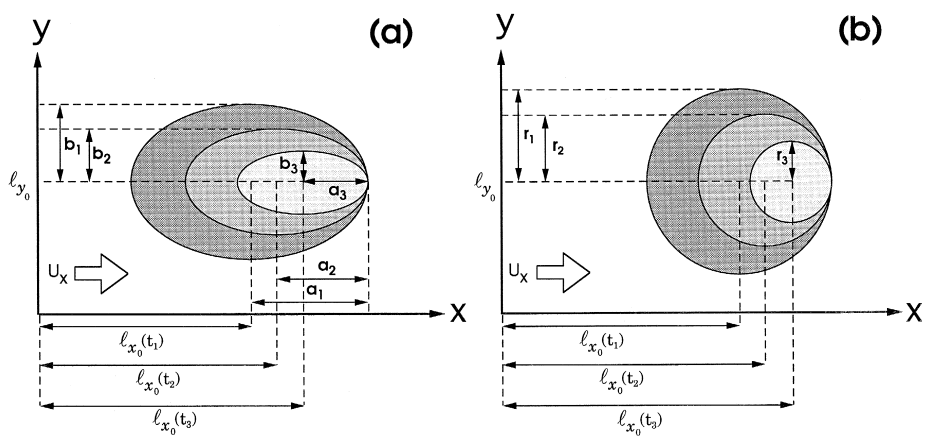

Fig. 3. Schematic illustration of (a) an elliptic and (b) a circular NAPL pool undergoing dissolution at three different times ($t_1 < t_2 < t_3$). As the dissolution process advances, the pool surface area shrinks, and the pool center shifts in the downstream direction. The x coordinate of the pool center, $\ell_{x_o}(t)$, increases in magnitude with time, whereas the y coordinate, $\ell_{y_o}(t)$, remains constant.

with the software PC-UNIFAC (BRI, 1993). The mole fraction, $X(t)$, of component p at time t is defined as

$$X_p(t) = \frac{\mathscr{M}_p(t)}{\sum_{p=1}^{\mathscr{P}} \mathscr{M}_p(t)} \qquad (p = 1,2,\ldots,\mathscr{P}), \tag{20}$$

where $\mathscr{P}$ is the total number of components in the nonaqueous phase; $\mathscr{M}_p(t)$ is the number of moles of component p present in the nonaqueous phase at time t given by

$$\mathscr{M}_p(t) = \mathscr{M}'_p - \sum_{m=1}^{m_f} \frac{k_p^* C_p^w(m\Delta t)\, A(m\Delta t)\,\theta\Delta t}{(\text{Mol wt})_p} \qquad (t \geq \Delta t), \tag{21}$$

where $\mathscr{M}'_p$ is the initial number of moles of component p in the nonaqueous phase; $A(t)$ is the pool surface area; θ is porosity; m is a summation index; m_f is an integer indicating the total number of time steps (or pulses), and is defined as: $m_f = \mathrm{I}(t/\Delta t)$ $(m_f = 1,2,3\ldots)$, where I ( ) is an integer mode arithmetic operator truncating off any fractional part of the numeric argument. The actual NAPL–water interfacial area is very difficult to determine because of the unknown pore-size distribution; however, in this study the time dependent NAPL–water interfacial area of the elliptic pool is described by

$$A(t) = \pi\, a(t)\, b(t). \tag{22}$$

Assuming that the ratio of major to minor semi-axis of the elliptic pool is equal to a time invariant parameter,

$$\xi = \frac{a(t)}{b(t)} = \text{const.}, \tag{23}$$

the time dependent coordinates of the pool center, as illustrated in Fig. 3a, are given by the following relationships

$$\ell_{x_o}(t) = \ell_{x_o}(t - \Delta t) + a(t - \Delta t) - a(t), \tag{24a}$$

$$\ell_{y_o}(t) = \ell_{y_o}(t - \Delta t). \tag{24b}$$

In view of Eqs. (22) and (23), the expression for $a(t)$ is

$$a(t) = \left[\frac{\xi A(t)}{\pi}\right]^{1/2}, \tag{25}$$

where the time-dependent pool surface area $A(t)$ is estimated by

$$A(t) = \sum_{p=1}^{\mathscr{P}} \frac{\mathscr{M}_p(t)(\text{Mol wt})_p}{\rho_p \theta d}, \tag{26}$$

where d is the thickness of the NAPL pool; and ρ_p is the liquid density of component p.

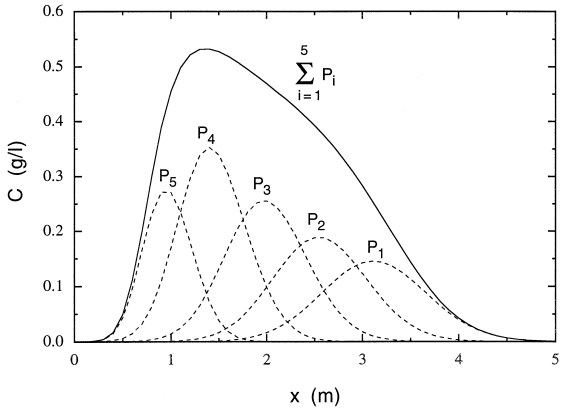

Fig. 4. Schematic of spatial liquid phase contaminant concentration distributions resulting from five consecutive pulse inputs (dashed curves) and overall concentration (solid curve) of a single component (1,1,2-TCA) elliptic pool (Here $a = 0.25$ m, $b = 0.18$ m, $\ell_{x_o} = 0.6m, \ell_{y_o} = 0.75m$, $t = 1000$ h, $\Delta t = 200$ h, $U_x = 3.1 \times 10^{-3}$ m/h, $y = 0.75$ m, $z = 0.1$ m).

The semi-analytical solution to the multicomponent dissolution problem is obtained by summing the aqueous phase concentrations resulting from all pulse-type inputs of equal duration Δt. For m_f pulses the desired expression is

$$C_p(t,x,y,z) = \sum_{m=1}^{m_f} \left[C_p^w(m\Delta t) - C_{b_p} \right] \times \left[\Phi_p(t-(m-1)\Delta t, x, y, z) - \Phi_p(t - m\Delta t, x, y, z) \right] + \left[C_p^w(m_f \Delta t) - C_{b_p} \right] \Phi_p(t - m_f \Delta t, x, y, z), \quad (27)$$

where $t - m_f \Delta t < \Delta t$. For each individual pulse, the parameter $\Phi(t,x,y,z)$ is evaluated by Eq. (14) with $C_p^w(t)$ obtained from Eq. (11) and $\ell_{x_o}(t)$ from Eq. (24a), as discussed above. A schematic illustration of the semi-analytical procedure applied to a hypothetical case of a single component NAPL elliptic pool (1,1,2-TCA) undergoing dissolution is presented in Fig. 4. The dashed curves represent aqueous phase concentration distributions for five consecutive pulses of equal duration and they are estimated by Eq. (13), whereas the solid curve corresponds to the total concentration estimated by Eq. (27) or by direct addition of the five concentration distributions presented.

3. Simulations and discussion

Consider three NAPL pools located at the bottom of a saturated, homogeneous sandy aquifer with unidirectional interstitial flow along the x-coordinate, as illustrated in Fig. 5. Pools 1 and 3 consist of uniform mixtures of 1,1,2-TCA and TCE, and Pool 2 consists only of TCE. Pool 1 is of elliptic shape whereas Pools 2 and 3 are of circular shape. All three pools have the same thickness $d = 0.003$ m. The exact initial pool coordinates,

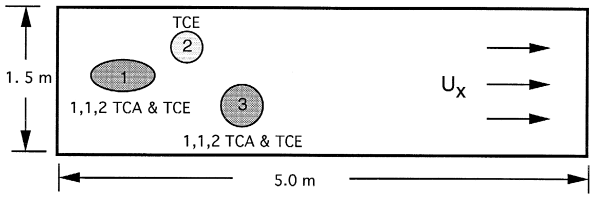

Fig. 5. Schematic illustration of the hypothetical aquifer and NAPL pools.

surface areas, and dimensions are presented in Table 1. It should also be noted that the initial mole fraction of the mixture in Pool 1 is 0.5 for both 1,1,2-TCA and TCE, and the initial mole fraction of the mixture in Pool 3 is 0.7 for 1,1,2-TCA and 0.3 for TCE. The model parameters employed for the simulations are listed in Table 2. The dispersion coefficients are calculated by the following relationships

$$D_x = \alpha_L U_x + \mathscr{D}_e, \tag{28a}$$

$$D_y = D_z = \alpha_T U_x + \mathscr{D}_e, \tag{28b}$$

where α_L and α_T are the longitudinal and transverse dispersivity, respectively. Furthermore, the porosity of the sandy aquifer is assumed to be $\theta = 0.3$, the interstitial fluid

Table 1
Initial physical description of NAPL pools

Parameter	Pool 1 (elliptic)	Pool 2 (circular)	Pool 3 (circular)
a (m)	0.253	–	–
A (m^2)	0.14	0.071	0.126
b (m)	0.176	–	–
d (m)	0.003	0.003	0.003
ℓ_{x_o} (m)	0.6	1.15	1.8
ℓ_{y_o} (m)	0.75	1.1	0.5
r (m)	–	0.15	0.2

Table 2
Parameter values for simulations

Parameter	1,1,2-TCA	TCE	Reference
C_b (g/l)	0.0	0.0	
C_s (g/l)	4.5	1.1	Mackay et al. (1992)
$\mathscr{D}_e$ (m^2/h)	2.33×10^{-6}	2.43×10^{-6}	Lee and Chrysikopoulos (1995)
D_x (m^2/h)	1.57×10^{-4}	1.57×10^{-4}	
D_y, D_z (m^2/h)	1.78×10^{-5}	1.79×10^{-5}	
k^* (m/h)	3.0×10^{-5}	3.0×10^{-5}	
Mol wt. (g/mol)	133.41	131.39	Mackay et al. (1992)
R	1.1	1.87	Lee and Chrysikopoulos (1995)
λ (h^{-1})	0.0	0.0	
ρ (g/m^3 at 20°C)	1.44×10^6	1.46×10^6	Mackay et al. (1992)

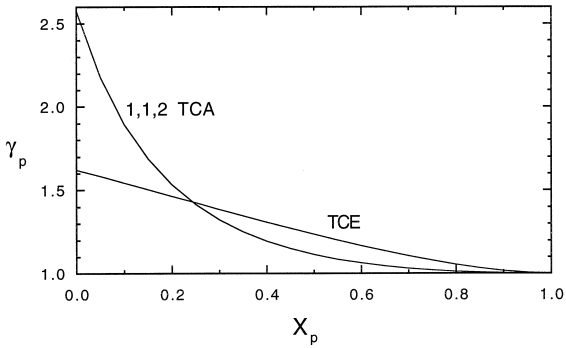

Fig. 6. Relationship between nonaqueous phase activity coefficients and component mole fractions for a 1,1,2-TCA and TCE mixture, as predicted by UNIFAC.

velocity $U_x = 3.1 \times 10^{-3}$ m/h, and the aquifer dispersivities $\alpha_L = 0.05$ m and $\alpha_T = 0.005$ m.

Concentration distributions for the two dissolving components within the sandy aquifer are predicted by the semi-analytical solution (Eq. (27)) in conjunction with the functional relationships between γ_p and X_p as predicted by UNIFAC (see Fig. 6). There are numerous advantages and benefits of the semi-analytical model presented in this work as compared with any numerical approximation. As described earlier, the present semi-analytical solution further advances modeling capabilities of currently available analytical solutions by adapting changes in each component's time-dependent equilibrium solubility as well as accounting for changes in source configuration. The required computational time of the semi-analytical solution is inversely proportional to the selected time step (Δt). It should be noted that the time step for which the equilibrium solubility of each pool component can be assumed to remain constant is subject to further experimental investigations. In this work, all simulations are conducted with $\Delta t = 200$ h. As the time step decreases, or equivalently, the number of pulses increases, the resolution of the semi-analytical model is enhanced. However, a larger time step will decrease the total number of pulses required per simulation, which in turn decreases the computational effort. Furthermore, the semi-analytical solution is not restricted by extensive memory and CPU requirements associated with numerical approximations, thus allows the possibility of obtaining three-dimensional simulations even on low-end personal computers.

Fig. 7 shows the equilibrium aqueous solubility of the components of each pool considered in this study, as a function of simulation time, predicted by Eq. (11). For Pools 1 and 3, $C^w_{1,1,2\text{-TCA}}$ is decreasing and C^w_{TCE} is increasing. The single component aqueous saturation concentration (solubility) for 1,1,2-TCA is 4.5 g/l and for TCE is 1.1 g/l (Mackay et al., 1992). Therefore, the mass of 1,1,2-TCA dissolving into the aqueous phase is greater than the TCE mass, leading to a lower 1,1,2-TCA mole fractions in Pools 1 and 3, and consequently, to higher 1,1,2-TCA nonaqueous phase activity coefficients. Clearly, $C^w_{1,1,2\text{-TCA}}$ decreases when the corresponding relative decrease in X is greater than the increase in γ. Similarly, the mass of TCE dissolving

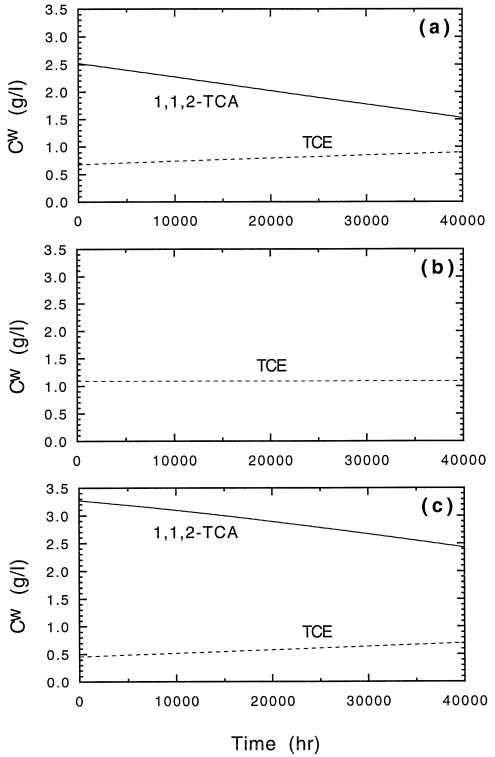

Fig. 7. Equilibrium aqueous solubility for (a) Pool 1, (b) Pool 2 and (c) Pool 3 as a function of simulation time.

into the aqueous phase is lower than the mass of 1,1,2-TCA, leading to higher TCE mole fractions, lower nonaqueous phase activity coefficients, and slowly increasing equilibrium aqueous solubilities. The general trend of the equilibrium aqueous solubility variation of 1,1,2-TCA and TCE is similar in both Fig. 7a and c; however, the equilibrium aqueous solubility values of each component of Pools 1 and 3 are not identical, because the two pools have different initial compositions. The equilibrium aqueous solubility for TCE in Pool 2 (Fig. 7b) is independent of time and equal to the TCE single component aqueous saturation concentration, because Pool 2 consist only of TCE.

Fig. 8 presents the number of moles of every component remaining in each pool as a function of simulation time, predicted by Eq. (21). As the simulation time increases, the number of moles of each component decreases due to the dissolution of the NAPL pools. However, the higher solubility of 1,1,2-TCA leads to faster reduction of the corresponding number of moles remaining in Pools 1 and 3 (see Fig. 8a,c). It should be noted that in Eq. (21), the time invariant overall mass transfer coefficient (k^*) is assigned the same value for both 1,1,2-TCA and TCE.

The change of the NAPL–water interfacial area as a function of simulation time for the three dissolving pools, as estimated by Eq. (26), are presented in Fig. 9. The rate of

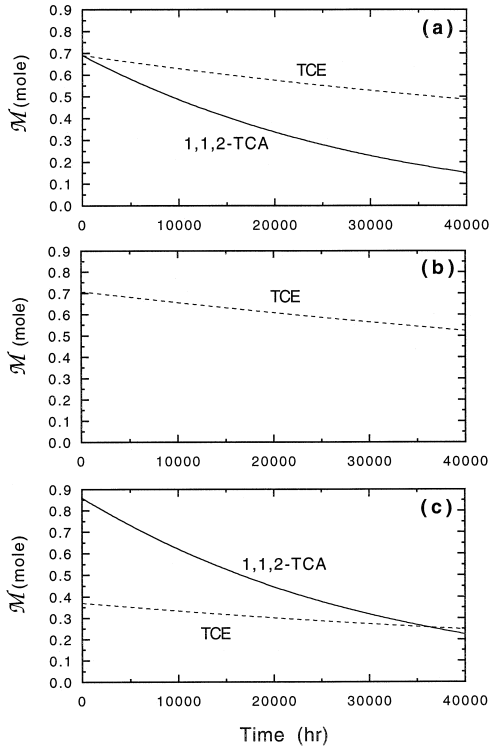

Fig. 8. Number of moles of 1,1,2-TCA and/or TCE remaining in (a) Pool 1, (b) Pool 2 and (c) Pool 3 as a function of simulation time.

shrinkage of Pool 1 is comparable to the rate of Pool 3, whereas the NAPL–water interfacial area of the single component (TCE) Pool 2 is reduced at a much slower rate. These results are relatively intuitive and in perfect agreement with those illustrated in Figs. 7 and 8.

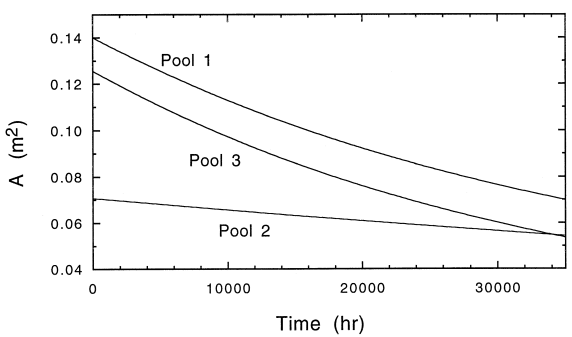

Fig. 9. Interfacial pool/water surface area as a function of simulation time for the three dissolving NAPL pools.

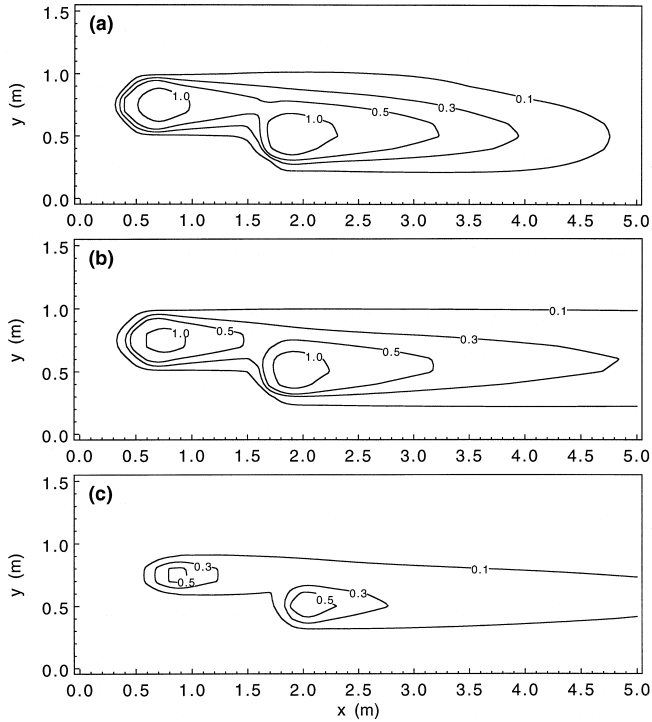

Fig. 10. Concentration contours in g/l of aqueous phase 1,1,2-TCA in the x,y plane at (a) 1000, (b) 5000, and (c) 30,000 h ($z = 0.01$ m).

Figs. 10 and 11 present x,y plane cross-sections of the plume resulted from the combined dissolution of the NAPL pools shown in Fig. 5, for 1,1,2-TCA and TCE, respectively. To illustrate the evolution of the plumes, snapshots at three different times since the initiation of the dissolution process are constructed. During early times (Fig. 10a,b as well as Fig. 11a,b), a steady increase in plume size is observed for both 1,1,2-TCA and TCE with increasing time. However, at late times (Fig. 10c and Fig. 11c), the concentration levels near the vicinity of the pools and throughout the aquifer all exhibit some progressive reduction, due to the shrinkage of the pools.

The importance of accounting for the changes in the nonaqueous phase activity coefficients during multicomponent NAPL pool dissolution is illustrated by the x,y plane contour plots for the aqueous phase concentrations of 1,1,2-TCA (Fig. 12a) and TCE (Fig. 12b). The solid contours represent concentrations in g/l, obtained with equilibrium aqueous solubilities estimated by Eq. (11) and nonaqueous activity coefficients calculated by UNIFAC. The dashed contours represent concentrations in g/l, obtained with equilibrium aqueous solubilities estimated by Raoult's law ($C_p^{\mathrm{w}} = C_{\mathrm{s}_p} X_p$). Comparison of the constructed contours indicate that the estimated contaminant concentrations may be quite different if γ_p is set to unity. It should be noted that the solid and dashed contours are indistinguishable for TCE concentrations near the vicinity of Pool 2, because this is a single component pool (see Fig. 12b).

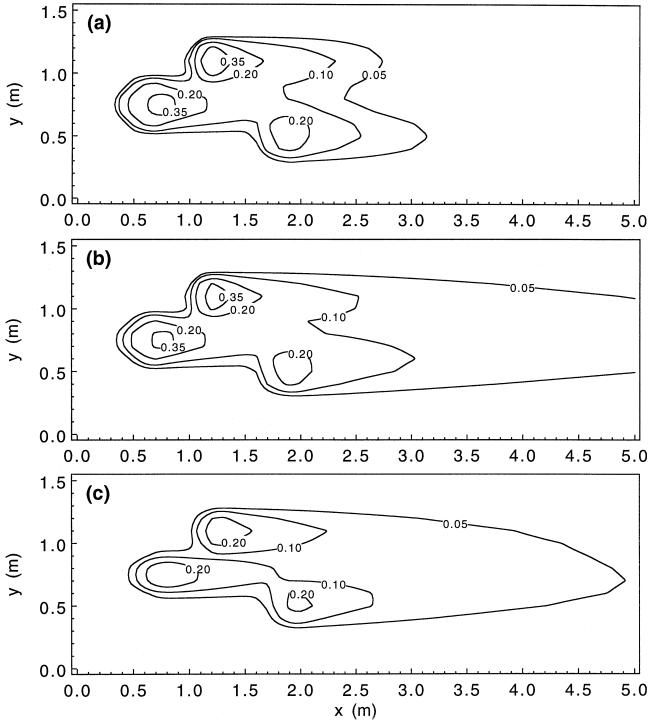

Fig. 11. Concentration contours in g/l of aqueous phase TCE in the x,y plane at (a) 1000, (b) 5000, and (c) 30,000 h ($z = 0.01$ m).

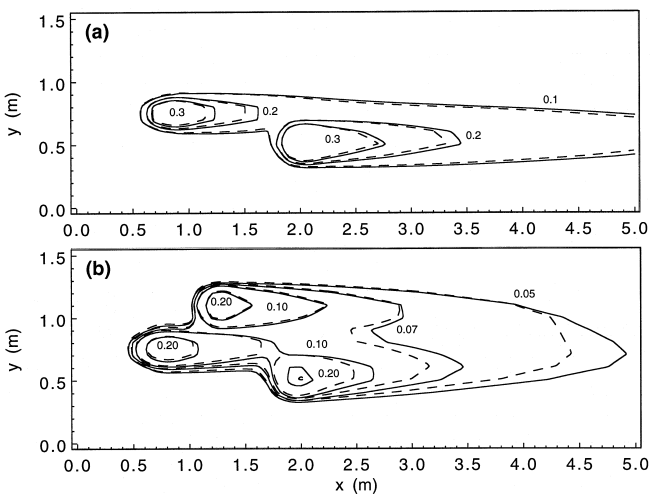

Fig. 12. Comparison between concentration contours in g/l in the x,y plane obtained with $\gamma_p = \gamma_p(X_p)$ (solid contours) and $\gamma_p = 1$ (dashed contours) for (a) 1,1,2-TCA and (b) TCE ($t = 30{,}000$ h, $z = 0.01$ m).

4. Summary

A model for contaminant transport originating from the dissolution of multicomponent NAPL pools in homogeneous, saturated three-dimensional subsurface formations is developed. The model assumes that the aqueous phase concentrations of the dissolved components are mass-transfer limited, and each dissolved component may undergo first-order decay and may sorb onto the solid matrix under local equilibrium conditions. A semi-analytical solution is obtained by summing the aqueous phase concentrations resulting from a series of short dissolution pulses. The equilibrium aqueous solubility of every pool constituent is estimated before the initiation of a pulse, and is considered constant for the duration of the pulse. The numerical code UNIFAC is employed for the evaluation of the time-dependent nonaqueous phase activity coefficients. The results from several synthetic examples demonstrate that failure to account for the changes in γ_p that take place during multicomponent dissolution, may lead to quite different results.

The model presented in this work is useful for the design and interpretation of experiments in laboratory bench scale aquifers, certain homogeneous subsurface formations, and for the verification of complex numerical codes. Although the model is limited to homogeneous field situations, it provides a starting point for investigating multicomponent NAPL pool dissolution problems.

5. Notation

a	Major semi-axis of elliptic pool, L.
A	Pool surface area, L^2.
b	Minor semi-axis of elliptic pool, L.
C	Liquid phase solute concentration(solute mass/liquid volume), M/L^3.
C_b	Background liquid phase solute concentration (solute mass/liquid volume), M/L^3.
C_s	Single component aqueous saturation concentration (solubility), M/L^3.
C^w	Equilibrium aqueous solubility, M/L^3.
d	Pool thickness, L.
$d^2\mathbf{A}$	Differential surface area.
$\mathscr{D}$	Molecular diffusion coefficient, L^2/t.
$\mathscr{D}_e$	Effective molecular diffusion coefficient, equal to $\mathscr{D}/\tau^*$, L^2/t.
D_x	Longitudinal hydrodynamic dispersion coefficient, L^2/t.
D_y	Lateral hydrodynamic dispersion coefficient, L^2/t.
D_z	Hydrodynamic dispersion coefficient in the vertical direction, L^2/t.
erf[x]	Error function, equal to $(2/\pi^{1/2})\int_0^x e^{-z^2}\mathrm{d}z$.
I( )	Integer mode arithmetic operator.
k	Local mass transfer coefficient, L/t.
$\bar{k}$	Average (or overall) mass transfer coefficient, L/t.
k^*	Time invariant overall mass transfer coefficient, L/t.

ℓ_{x_o}, ℓ_{y_o}	x and y Cartesian coordinates respectively, of the center of an elliptic/circular pool, L.
m	Summation index.
m_f	Total number of time steps.
$\mathscr{M}$	Number of moles remaining in a pool, mol.
$\mathscr{M}'$	Initial number of moles in a pool, mol.
n_1, n_2	Defined in Eqs. (17) and (18), respectively.
p	Component number indicator.
$\mathscr{P}$	Total number of components.
r	Radius of circular pool, L.
R	Dimensionless retardation factor.
t	Time, t.
U_x	Average interstitial velocity, L/t.
v	Defined in Eq. (19).
x, y, z	Spatial coordinates, L.
X	Dimensionless mole fraction.

Greek letters

α_L, α_T	Longitudinal and transverse dispersivity, respectively, L.
γ	Dimensionless activity coefficient.
Δt	Time interval of a single pulse.
θ	Porosity (liquid volume/aquifer volume), L^3/L^3.
λ	Decay coefficient, t^{-1}.
μ	Dummy integration variable.
μ_1, μ_2	Defined in Eqs. (15) and (16), respectively.
ξ	Ratio of major to minor semi-axis of elliptic pool.
ρ	Liquid density, M/L^3.
τ	Dummy integration variable.
τ^*	Tortuosity factor (≥ 1).
Φ	Defined in Eq. (14).

Abbreviations

NAPL	Nonaqueous phase liquid
1,1,2-TCA	1,1,2-trichloroethane
TCE	Trichloroethylene
UNIFAC	UNI-Functional group Activity Coefficients

Acknowledgements

This research was sponsored by the Environmental Protection Agency, under Grant No. R-823579-01-0. However, the manuscript has not been subjected to the Agency's peer and administrative review and therefore does not necessarily reflect the views of the Agency, and no official endorsement should be inferred. The authors acknowledge Youn Sim and Tae-Joon Kim for many stimulating discussions.

References

Abriola, L.M., Pinder, G.F., 1985. A multiphase approach to the modeling of porous media contamination by organic compounds: 1. Equation development. Water Resour. Res. 21, 11–18.

Anderson, M.R., Johnson, R.L., Pankow, J.F., 1992. Dissolution of dense chlorinated solvents into groundwater: 3. Modeling contaminant plumes from fingers and pools of solvent. Environ. Sci. Technol. 26, 901–908.

Banerjee, S., 1984. Solubility of organic mixtures in water. Environ. Sci. Technol. 18, 587–591.

Batu, V., 1996. A generalized three-dimensional analytical solute transport model for multiple rectangular first-type sources. J. Hydrol. 174, 57–82.

Bird, R.B., Stewart, W.E., Lightfoot, E.N., 1960. Transport Phenomena. Wiley, New York, 780 pp.

Borden, R.C., Piwoni, M.D., 1992. Hydrocarbon dissolution and transport: A comparison of equilibrium and kinetic models. J. Contam. Hydrol. 10, 309–323.

Bosma, W.J.P., van der Zee, S.E.A.T.M., van Duijn, C.J., 1996. Plume development of a nonlinearly adsorbing solute in heterogeneous porous formations. Water Resour. Res. 32, 1569–1584.

BRI, 1993. PC-UNIFAC-4.0. P.O. Box 7834, Atlanta, GA 30357-0834.

Broholm, K., Feenstra, S., 1995. Laboratory measurements of the aqueous solubility of mixtures of chlorinated solvents. Environ. Toxicol. Chem. 14, 9–15.

Chrysikopoulos, C.V., 1995. Three-dimensional analytical models of contaminant transport from nonaqueous phase liquid pool dissolution in saturated subsurface formations. Water Resour. Res. 31, 1137–1145.

Chrysikopoulos, C.V., Voudrias, E.A., Fyrillas, M.M., 1994. Modeling of contaminant transport resulting from dissolution of nonaqueous phase liquid pools in saturated porous media. Transp. Porous Media 16, 125–145.

Crank, J., 1975. The Mathematics of Diffusion. Oxford Press, Great Britain, 414 pp.

Fredenslund, A., Jones, R.L., Prausnitz, J.M., 1975. Group-contribution estimation of activity coefficients in nonideal liquid mixtures. AIChE J. 21, 1086–1099.

Fredenslund, A., Gmehling, J., Rasmussen, P., 1977. Vapor–liquid Equilibria Using UNIFAC, Elsevier, New York, 380 pp.

Geller, J.T., Hunt, J.R., 1993. Mass transfer from nonaqueous phase organic liquids in water-saturated porous media. Water Resour. Res. 29, 833–845.

Gmehling, J., Rasmussen, P., Fredenslund, A., 1982. Vapor–liquid equilibria by UNIFAC group contribution: 2. Revision and extension. Ind. Eng. Chem. Process Des. Dev. 21, 118–127.

Goltz, M.N., Roberts, P.V., 1986. Three-dimensional solutions for solute transport in an infinite medium with mobile and immobile zones. Water Resour. Res. 22, 1139–1148.

Hansen, H.K., Rasmussen, P., Fredenslund, A., Schiller, M., Gmehling, J., 1991. Vapor–liquid equilibria by UNIFAC group contribution: 5. Revision and extension. Ind. Eng. Chem. Res. 30, 2352–2355.

Holman, H.-Y.N., Javandel, I., 1996. Evaluation of transient dissolution of slightly water-soluble compounds from a light nonaqueous phase liquid pool. Water Resour. Res. 32, 915–923.

Hunt, B., 1978. Dispersive sources in uniform groundwater flow. J. Hydraul. Div. Am. Soc. Civ. Eng. 104, 75–85.

Imhoff, P.T., Jaffé, P.R., Pinder, G.F., 1994. An experimental study of complete dissolution of a nonaqueous phase liquid in saturated porous media. Water Resour. Res. 30, 307–320.

Incropera, F.P., DeWitt, D.P., 1990. Fundamentals of Heat and Mass Transfer, 3rd edn., Wiley, New York, 919 pp.

Johnson, R.L., Pankow, J.F., 1992. Dissolution of dense chlorinated solvents into groundwater: 2. Source functions for pools of solvent. Environ. Sci. Technol. 26, 896–901.

Kan, A.T., Tomson, M.B., 1996. UNIFAC prediction of aqueous and nonaqueous solubilities of chemicals with environmental interest. Environ. Sci. Technol. 30, 1369–1376.

Lee, K.Y., Chrysikopoulos, C.V., 1995. Numerical modeling of three-dimensional contaminant migration from dissolution of multicomponent NAPL pools in saturated porous media. Environ. Geology 26, 157–165.

Leij, F.J., Skaggs, T.H., van Genuchten, M.Th., 1991. Analytical solutions for solute transport in three-dimensional semi-infinite porous media. Water Resour. Res. 27, 2719–2733.

Leij, F.J., Toride, N., van Genuchten, M.Th., 1993. Analytical solutions for non equilibrium solute transport in three-dimensional porous media. J. Hydrol. 151, 193–228.

Lenhard, R.J., Johnson, T.G., Parker, J.C., 1993. Experimental observations of nonaqueous phase liquid subsurface movement. J. Contam. Hydrol. 12, 79–101.

Lingineni, S., Dhir, V.K., 1997. Controlling transport processes during NAPL removal by soil venting. Adv. Water Resour. 20, 157–169.

Macedo, E.A., Weidlich, U., Gmehling, J., Rasmussen, P., 1983. Vapor–liquid equilibria by UNIFAC group contribution: 3. Revision and extension. Ind. Eng. Chem. Process Des. Dev. 22, 676–684.

Mackay, D., Shiu, W.Y., Maijanen, A., Feenstra, S., 1991. Dissolution of non-aqueous phase liquids in groundwater. J. Contam. Hydrol. 8, 23–42.

Mackay, D., Shiu, W.Y., Ma, K.C., 1992. Illustrated Handbook of Physical-chemical Properties and Environmental Fate for Organic Chemicals, Vol. 3. Volatile Organic Chemicals. Lewis Publishers, Chelsea, MI, 916 pp.

Mason, A.R., Kueper, B.H., 1996. Numerical simulation of surfactant-enhanced solubilization of pooled DNAPL. Environ. Sci. Technol. 30, 3205–3215.

Mayer, A.S., Miller, C.T., 1996. The influence of mass transfer characteristics and porous media heterogeneity on nonaqueous phase dissolution. Water Resour. Res. 32, 1551–1567.

Munz, C., Roberts, P.V., 1987. Air–water phase equilibria of volatile organic solutes. J. Am. Water Works Assoc. 79, 62–69.

Pantazidou, M., Sitar, N., 1993. Emplacement of non-aqueous liquids in the vadose zone. Water Resour. Res. 29, 705–722.

Pearce, A.E., Voudrias, E.A., Whelan, M.P., 1994. Dissolution of TCE and TCA pools in saturated subsurface systems. J. Environ. Eng. ASCE 120, 1191–1206.

Powers, S.E., Abriola, L.M., Weber, W.J., 1994. An experimental investigation of nonaqueous phase liquid dissolution in saturated subsurface systems: Transient mass transfer rates. Water Resour. Res. 30, 321–332.

Seagren, E.A., Rittmann, B.E., Valocchi, A.J., 1994. Quantitative evaluation of the enhancement of NAPL–pool dissolution by flushing and biodegradation. Environ. Sci. Technol. 28, 833–839.

Schwarzenbach, R.P., Gschwend, P.M., Imboden, D.M., 1993. Environ. Organic Chem. Wiley, New York, 681 pp.

Schwille, F., 1988. Dense Chlorinated Solvents in Porous and Fractured Media, Translated by J.F. Pankow. Lewis, Chelsea, MI, 146 pp.

Skjold-Jørgensen, S., Kolbe, B., Gmehling, J., Rasmussen, P., 1979. Vapor–liquid equilibria by UNIFAC group contribution: Revision and extension. Ind. Eng. Chem. Process Des. Dev. 18, 714–722.

Tiegs, D., Gmehling, J., Rasmussen, P., Fredenslund, A., 1987. Vapor-liquid equilibria by UNIFAC group contribution: 4. Revision and extension. Ind. Eng. Chem. Process Des. Dev. 26, 159–161.

Voudrias, E.A., Yeh, M.F., 1994. Dissolution of a toluene pool under constant and variable hydraulic gradients with implications for aquifer remediation. Groundwater 32, 305–311.

Weber Jr., W.J., DiGiano, F.A., 1996. Process Dynamics in Environmental Systems. Wiley-Interscience, New York, 493 pp.

Whelan, M.P., Voudrias, E.A., Pearce, A., 1994. DNAPL pool dissolution in saturated porous media: Procedure development and preliminary results. J. Contam. Hydrol. 15, 223–237.

Wilson, J.L., Miller, P.J., 1978. Two-dimensional plume in uniform groundwater flow. J. Hydraul. Div. Am. Soc. Civ. Eng. 104, 503–514.